



HAL
open science

Ultrahigh vacuum Raman spectroscopy for the preparation of III–V semiconductor surfaces

Wijden Khelifi, Damien Canneson, Maxime Berthe, Sébastien Legendre, Christophe Coinon, Ludovic Desplanque, Xavier Wallart, Louis Biadala, Bruno Grandidier, Pierre Capiod

► **To cite this version:**

Wijden Khelifi, Damien Canneson, Maxime Berthe, Sébastien Legendre, Christophe Coinon, et al.. Ultrahigh vacuum Raman spectroscopy for the preparation of III–V semiconductor surfaces. *Review of Scientific Instruments*, 2023, 94 (12), 10.1063/5.0152031 . hal-04349101v2

HAL Id: hal-04349101

<https://hal.science/hal-04349101v2>










Submitted on 2 Dec 2024

HAL is a multi-disciplinary open access archive for the deposit and dissemination of scientific research documents, whether they are published or not. The documents may come from teaching and research institutions in France or abroad, or from public or private research centers.

L'archive ouverte pluridisciplinaire **HAL**, est destinée au dépôt et à la diffusion de documents scientifiques de niveau recherche, publiés ou non, émanant des établissements d'enseignement et de recherche français ou étrangers, des laboratoires publics ou privés.

RESEARCH ARTICLE | DECEMBER 05 2023

Ultrahigh vacuum Raman spectroscopy for the preparation of III–V semiconductor surfaces

Wijden Khelifi ; Damien Cannesson ; Maxime Berthe ; Sébastien Legendre ; Christophe Coinon ; Ludovic Desplanque ; Xavier Wallart ; Louis Biadala ; Bruno Grandidier ; Pierre Capiod 



Rev. Sci. Instrum. 94, 123702 (2023)

<https://doi.org/10.1063/5.0152031>



View
Online



Export
Citation

Articles You May Be Interested In

Development of a combined portable x-ray fluorescence and Raman spectrometer for *in situ* analysis

Rev. Sci. Instrum. (June 2014)

Single lateral mode mid-infrared laser diode using wavelength-scale modulation of the facet reflectivity

Appl. Phys. Lett. (January 2012)

Direct measurement of band offsets on selective area grown $\text{In}_{0.53}\text{Ga}_{0.47}\text{As}/\text{InP}$ heterojunction with multiple probe scanning tunneling microscopy

Appl. Phys. Lett. (November 2022)



Special Topics Open
for Submissions

[Learn More](#)

Ultrahigh vacuum Raman spectroscopy for the preparation of III–V semiconductor surfaces

Cite as: Rev. Sci. Instrum. 94, 123702 (2023); doi: 10.1063/5.0152031

Submitted: 27 March 2023 • Accepted: 9 November 2023 •

Published Online: 5 December 2023













View Online



Export Citation



CrossMark

Wijden Khelifi,¹  Damien Canneson,^{1,2}  Maxime Berthe,¹  Sébastien Legendre,² 
Christophe Coinon,¹  Ludovic Desplanque,¹  Xavier Wallart,¹  Louis Biadala,¹ 
Bruno Grandidier,¹  and Pierre Capiod^{1,a)} 

AFFILIATIONS

¹ University Lille, CNRS, Centrale Lille, University Polytechnique Hauts-de-France, Junia-ISEN, UMR 8520 - IEMN, F-59000 Lille, France

² HORIBA France SAS, 455 Avenue Eugène Avinée 59120 Loos, Avenue de la Vauve–Passage Jobin Yvon, 91120 Palaiseau, France

^{a)} Author to whom correspondence should be addressed: pierre.capiod@junia.com

ABSTRACT

Raman spectroscopy is well-suited for the characterization of semiconductor materials. However, due to the weakness of the Raman signal, the studies of thin semiconductor layers in complex environments, such as ultrahigh vacuum, are rather scarce. Here, we have designed a Raman apparatus based on the use of a fiber optic probe, with a lens collecting the backscattered light directly inserted in ultrahigh vacuum. The solution has been tested for the preparation of III–V semiconductor surfaces, which requires the recovery of their atomic reconstruction. The surfaces were either protected with a thin As amorphous layer or covered with a native oxide prior to their treatment. The analysis of the Raman spectra, which was correlated with the study of the surfaces with low temperature scanning tunneling microscopy at the end of the cleaning process, shows the high potential of Raman spectroscopy for monitoring the cleanliness of III–V semiconductor heterostructures *in situ*.

Published under an exclusive license by AIP Publishing. <https://doi.org/10.1063/5.0152031>

I. INTRODUCTION

Raman spectroscopy is an analysis technique based on the inelastic scattering of monochromatic light from phonons in materials. When applied to semiconductor materials, it provides invaluable qualitative and quantitative information, such as their crystal structure, chemical composition, strain, doping level, and the nature of their defects.^{1–3} However, Raman scattering is a very weak effect. If the volume of the materials reduces to a few layers, the response signal becomes even smaller, making the use of this non-invasive spectroscopic technique more delicate for the analysis of semiconductor surfaces or ultra-thin materials. It requires the design of specific optics that are efficient enough to collect photons undergoing inelastic scattering. Despite successful examples of Raman analysis of few-layer semiconductor materials for the past decade,^{4–9} many semiconductors suffer from a significant surface reactivity. As a result, upon air-exposure, they lose their intrinsic properties,

precluding a Raman analysis under ambient conditions. Conversely, the ultrahigh vacuum (UHV) environment preserves the cleanliness and the crystal structure of semiconductor surfaces and subsurface layers. It is compatible with most of the vapor phase growth methods. However, it imposes additional constraints to maximize light collection and overcome the competing phenomenon of fluorescence induced by the surrounding of the sample. Solving all these issues has been essential in the understanding of the reconstructions at semiconductor surfaces^{10,11} and the development of novel two-dimensional materials, such as silicene and borophene, which are unstable in air environment.^{12,13} Among the existing Raman spectroscopic tools,^{14–20} fiber Raman probes, which combine Raman spectroscopy and fiber optics technology, are usually designed to perform minimally invasive analyses of hardly accessible samples. Here, we report on the development of such a fiber probe for the surface preparation of III–V compounds. Usually, III–V semiconductors are covered by a thin native oxide layer, which can be

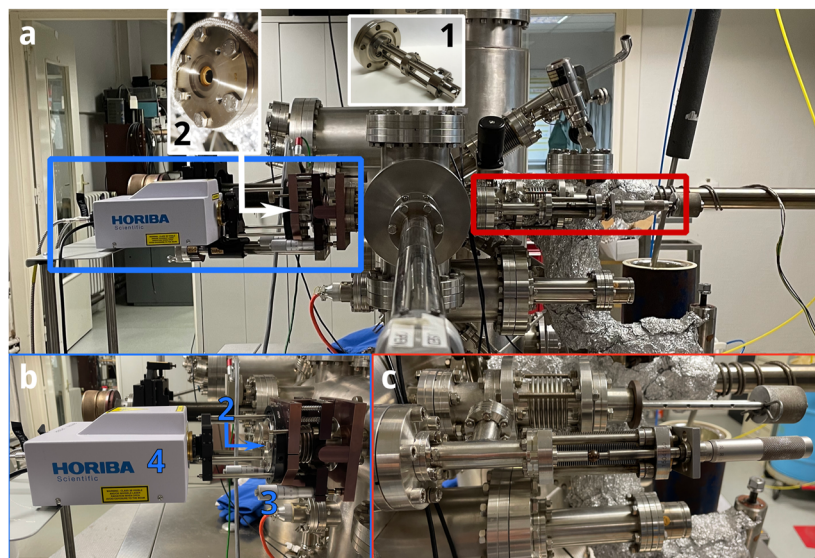


FIG. 1. (a) Photograph of the whole Raman system attached to the UHV preparation chamber of a commercially available low-temperature STM. The left part (blue rectangle) is dedicated to the optical pathways, while the right part (red rectangle) consists of a linear shift to translate the sample toward the lens. (b) Zoom of the left part where the Horiba SuperHead (element 4) is connected to the cage system (element 3) tightened to the viewport (element 2). (c) Zoom of the right part showing the linear shift. Inset 1 is the photograph of the optical UHV lens system, which is screwed to CF-40 flange viewport shown in a magnified view in inset 2. The white and blue arrows point the position of the viewport on the system.

removed in UHV by thermal annealing under a flux of group V elements^{21,22} or a flux of atomic hydrogen.^{23,24} However, clean and well-ordered III–V surfaces can also be protected by an amorphous capping layer, which can be further sublimated once the sample has been processed and transferred to another UHV system.^{25,26} By correlating the optical data measured with Raman spectroscopy with the topography of several III–V semiconductor surfaces obtained with low temperature scanning tunneling microscopy (STM), we show that Raman spectroscopy can be used to monitor the surface preparation and provides fast and direct information of the quality of the processed surfaces.

II. TECHNICAL DETAILS

A. Experimental setup

The use of optical fibers to deliver light to and from the sample was key to taking Raman spectroscopy out of conventional light microscopy. Current online Raman analysis can be performed, thanks to the use of fiber optic probes installed remotely, under relatively demanding and hostile conditions, while the analyzer itself remains in a controlled and safe environment. Although fiber optic probes include optimized optical components, none of them has been designed to withstand the constraints of growth conditions of advanced materials in high or ultrahigh vacuum (UHV): pressures in the 10^{-10} mbar range, bake out of the system up to 180 °C, and antifouling system to protect the sampling optics. Therefore, *ex situ* fiber optic probes are used for laser focusing on the sample and the collection of Raman scattered light, while additional optics must be developed to be inserted between the optic probe and the sample prepared in UHV. A photograph of the whole Raman

setup is shown in Fig. 1(a). The left part (blue rectangle) consists of the optical pathways with the incident laser beam and the reflected Raman signal. The right part (red rectangle) is the linear translation to approach the sample toward the lens (see below for details).

Based on our previous design, which provided a tube terminated with a lens to bring and collect the light from a sample in UHV,²⁷ a new version of the optics has been developed as shown in inset 1 of Fig. 1. The lens (AL108-B, Thorlabs) is not used anymore as a viewport between the UHV environment and the air but, instead, maintained in UHV. As a result, its diameter can be increased to 10 mm and the working distance reduced to 6 mm. Hence, a higher numerical aperture (NA) can be achieved. As NA depends on the diameter of the excitation and collection beams, corresponding to 6 mm, an effective NA of 0.4 is achieved (instead of 0.1 for the previous design), enhancing the collection of photons significantly. The lens is attached to the outer ring of a cylindrical cage consisting of three protruding metallic rods inserted into three rings that ensure the rigidity of the cage. The third ring is screwed to a homemade (DN40) CF-flanged viewport, which is mounted on the preparation chamber of an UHV system, including a low temperature scanning tunneling microscope (Omicron). This viewport consists of a wedge window (WW10530, Thorlabs), which is sealed to the flange with an UHV proof bi-component epoxy glue (inset 2 of Fig. 1, a white arrow points the position of the viewport on the whole system).

This flange is used to attach a mechanical system that anchors the fiber probe (SuperHead, Horiba) [element 4, Fig. 1(b)]. As a result, the SuperHead and the lens are tightened together and well aligned. The viewport [element 2, Fig. 1(b)], which is decoupled

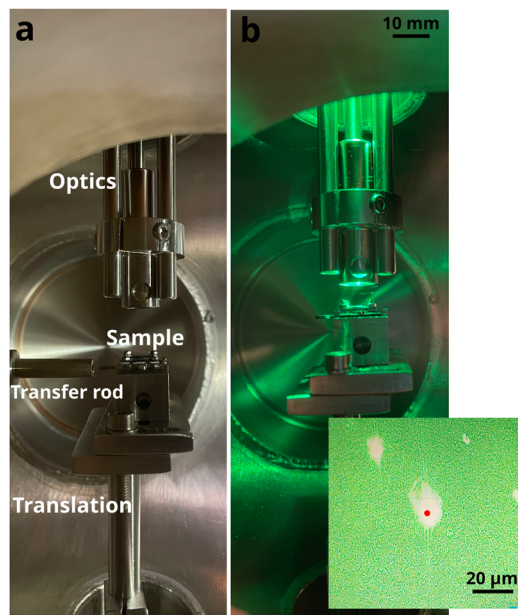


FIG. 2. (a) Photograph of the sample stage and the optics in UHV. A sample is inserted in the sample stage with the transfer rod seen to the left. (b) Photograph with the laser hitting the sample. Inset: Photograph of the camera with the laser beam focused onto the sample surface. Additional reflections are seen coming from the ion gauge of the UHV chamber.

from the preparation chamber by a bellow, can then be manipulated with a port aligner [element 3, Fig. 1(b)]. Micrometer screws are used to adjust the beam directions coming out from the SuperHead, allowing to probe different areas on the sample. Two optical fibers are connected at the rear of the Horiba SuperHead, one for the incident beam and the other for the reflected beam. The focus is achieved by adjusting the position of the sample in the UHV chamber, thanks to a linear translation seen in the red rectangle of Fig. 1(c). A camera is integrated in the SuperHead, which is helpful to adjust the sample to the focal point. Alternatively, one can adjust the position by maximizing the Raman signal in the analyzer. The translation of the sample is composed of a rod compensating a bellow, and the length of the bellow is adjusted with a micrometer screw for precision positioning of the sample inside the UHV chamber. The sample is held by a stage with a geometry suitable to welcome standard flag-style sample plates. The sample is inserted into the sample slot using a magnetic transfer rod. Figure 2(a) shows the UHV environment where the sample inserted in the stage is far from the lens. By adjusting the position of the sample stage, thanks to the micrometer screw, the sample can be brought close to the UHV lens as demonstrated on the photograph shown in Fig. 2(b). With the help of the camera integrated with the SuperHead, the sample can be easily focused. A photograph of the camera view is displayed in the inset of Fig. 2(b). The red dot corresponds to the middle of the laser target. The halo around is the reflection of the laser hitting the sample surface.

The optics in the fiber optic probe is optimized to work at a wavelength of 532 nm. The probe is composed of mirrors, ensuring a good alignment of the excitation and collection paths, and filters for the separation of the Raman signal from the excitation. While the laser source can deliver up to 250 mW, the measured laser power on the sample was in the range of a few mW to 10 mW at most. Based on the design of the apparatus, the scattered light is collected in a backscattering configuration. The fiber optic probe is coupled to a spectrometer (iHR 320, Horiba) through a multimode fiber. In the spectrometer, the light is dispersed by a grating (1200 grooves/mm) and then detected with a CCD camera thermoelectrically cooled to -60°C (Syncerity, Horiba). The acquisition time and accumulation pass are set to improve the signal to noise ratio. A typical timeframe for the measurement of a spectrum is around 5 min. The whole system provides a cutoff wave number of 60 cm^{-1} .

B. Samples

To investigate the surface preparation of III-V semiconductor materials, four different samples were grown by molecular beam epitaxy (MBE) in a RIBER Compact 21 system equipped with valved cracker cells for As and Sb evaporation. The first one consisted of a 30 nm-thick $\text{In}_{0.53}\text{Ga}_{0.47}\text{As}$ quantum well grown by molecular beam epitaxy (MBE) on a Zn-doped InP (001) substrate with a concentration of $4 \times 10^{18}\text{ cm}^{-3}$. The growth temperature was set at 490°C . The flux of In and Ga was 0.2 monolayer per second (ML/s), and the flux of As_4 was 1.2 ML/s. At the end of the growth, the surface was capped with amorphous arsenic to prevent its oxidation during air exposure.²⁸ For that purpose, the As layer was deposited at 15°C for 15 min with an As_4 flux of 4.5 ML/s. As the light penetration depth at a wavelength of 532 nm is much larger than the thickness of the $\text{In}_{0.53}\text{Ga}_{0.47}\text{As}$ quantum well,²⁹ the underlying InP substrate is expected to contribute to the Raman signal. Therefore, a Zn-doped InP (001) substrate was also considered as a reference. For this sample, the InP native oxide layer of the substrate was removed by thermal annealing at 400°C under a combination of arsenic and atomic hydrogen flux in the MBE chamber. The InP (001) surface was subsequently covered with a similar amorphous arsenic capping layer, using the conditions described above.

After the MBE growth, both samples were briefly exposed to air to be transferred into a vacuum vessel. Then, they were carried to the remote UHV system hosting the fiber optic probe for Raman spectroscopy. Their transfer to the load lock of the UHV system requires a brief exposure to air again. Once loaded into the preparation chamber of the UHV system, the samples were first characterized with Raman spectroscopy. The samples were subsequently annealed via radiative heating at 330°C , slightly higher than the threshold temperature of 270°C .³⁰ The temperature was controlled with a thermocouple connected near the back of the sample holder. During the sublimation of the 20-nm thick capping layer, the presence of As species in the chamber was measured using a mass spectrometer. Raman spectroscopy was always performed at room temperature as the sample stage for Raman analysis did not have any heating capabilities.

The third sample was grown on a Te-doped InSb (001) substrate with a concentration of $4 \times 10^{17}\text{ cm}^{-3}$. It consisted of a

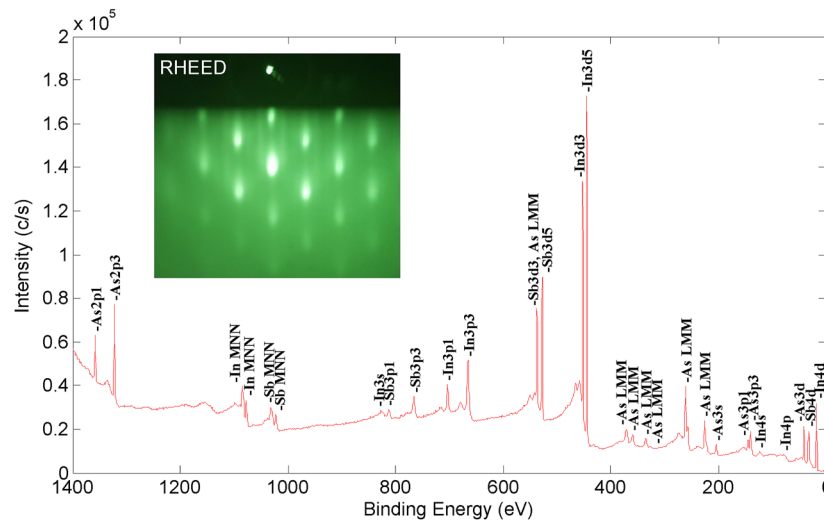


FIG. 3. XPS survey analysis of a reconstructed InSb(001) sample after the sublimation of an amorphous As layer. As species are still present in the survey spectrum. Inset: reflection high energy electron diffraction of the surface after annealing and uncapping of the As amorphous layer.

stack of three layers: an InSb buffer layer with a thickness of 20 nm, a 10 nm-thick $\text{Al}_{0.3}\text{In}_{0.7}\text{Sb}$ barrier, and, on top, a 30 nm-thick InSb quantum well. The quantum well was grown at 390°C using In and Sb fluxes of 0.2 and 2 ML/s, respectively. The fourth sample was a 30 nm-thick InSb quantum well grown by MBE on an S-doped InP (111) substrate. The sample preparation included two steps. The InP surface was first deoxidized under an As_4 atmosphere raising the temperature up to 500°C . During this process, an exposure to atomic hydrogen was performed for 30 s at the temperature of 200°C . Then, the InSb growth occurred at 390°C using In and Sb fluxes of 0.05 and 6 ML/s, respectively.

An attempt to cover the InSb surfaces with a protective amorphous arsenic layer was performed. However, after the sublimation of the As capping layer, the analysis of the reconstructed surface with x-ray photoemission spectroscopy revealed the presence of As species on the surface (see Fig. 3), indicating that arsenic had replaced antimony, consistent with the literature.³¹ In order to avoid the formation of a ternary alloy at the surface of the InSb quantum wells, which would make the interpretation of the Raman spectra more complex, the InSb surfaces were not protected and became, therefore, oxidized during their short transfer in air. The removal of the oxide layer was performed by simultaneously annealing the sample at 200°C and eroding the surface with atomic hydrogen bombardment. The bombardment was performed at a pressure of 4×10^{-6} mbar using an ISE10 ion gun (Scienta Omicron) connected to a hydrogen gas line.

III. RESULTS

A. InGaAs/InP heterostructure

High-quality surfaces of III–V semiconductor are key to interfacing materials and making devices. For example, clean and recon-

structed surfaces are required to reach a homogeneous nucleation in selective area heteroepitaxy of in-plane III–V nanowires.³² They are also beneficial to the controlled growth of high-k layers with atomic layer deposition.³³ Similarly, by minimizing the density of defective interfacial bonds in the fabrication of metal contacts, good electrical properties with negligible leakage currents can be obtained.³⁴ This is particularly true for InGaAs, which is a ternary compound semiconductor. Thanks to a lattice-matched growth on the InP substrate, it is commonly used as a conductive channel for high-frequency III–V metal–oxide–semiconductor field effect transistors (MOSFETs).³⁵ Owing to its direct bandgap, which can be varied over a significant energy range by changing the In mole fraction, it is a prime material for telecommunication with emission wavelengths between 1.3 and $1.6 \mu\text{m}$.^{36–38} To obtain high-quality InGaAs surfaces, the material can be protected with a thin As amorphous capping layer at the end of the growth. Its annealing in UHV around 350°C leads to the sublimation of the As layer and allows us to recover the reconstructed surfaces.^{39,40} To test the ability of Raman spectroscopy in monitoring the desorption of the As layer, the sublimation of the As layer was investigated first for the reference InP substrate and then for the $\text{In}_{0.53}\text{Ga}_{0.47}\text{As}$ quantum well.

The Raman spectra measured before the sublimation of the 30-nm thick As capping layer for the InP substrate and the $\text{In}_{0.53}\text{Ga}_{0.47}\text{As}$ quantum well are shown in Figs. 4(a) and 4(b), respectively. Both spectra look similar. An intense doublet is observed between 170 and 270 cm^{-1} . This peak is surrounded by additional small peaks and a shoulder at low (108 and 133 cm^{-1}) and high (278 cm^{-1}) wave numbers, respectively. All these features are typical of the modes measured with Raman spectroscopy on bulk amorphous arsenic^{41,42} and attest of the presence of an As capping layer. An additional broad peak extending between 410 and 520 cm^{-1} is also measured. We attribute it to the overtone of the doublet peak.

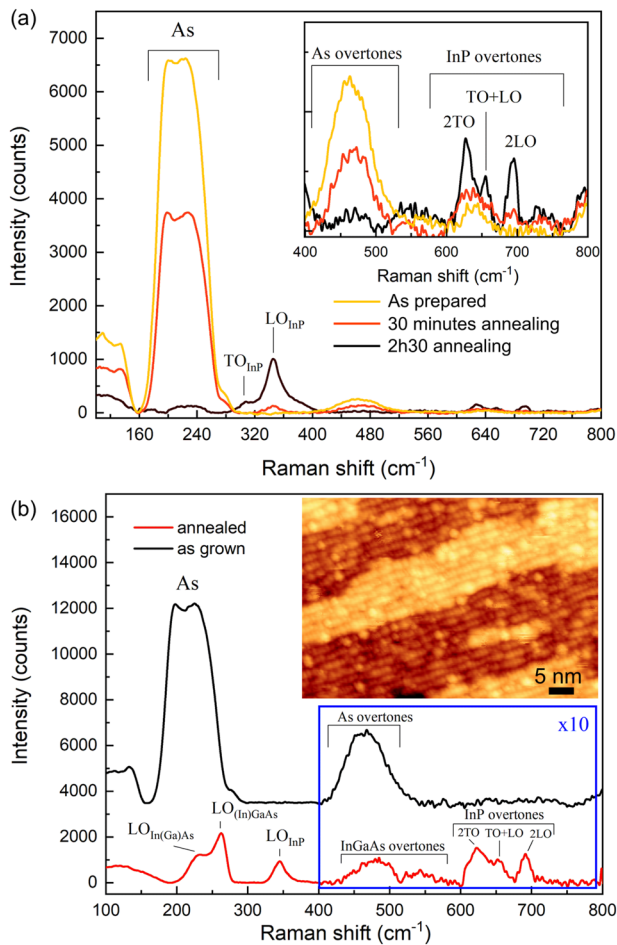


FIG. 4. (a) Evolution of the Raman spectra measured on an As-capped InP (001) substrate upon annealing at 330 °C first for 30 min and then for 2 more h. The transverse and longitudinal optical phonon modes are labeled TO and LO, respectively. The phonon lines related to amorphous arsenic are labeled As. Inset: amplified signal in the spectral region of the overtones. (b) Raman spectra measured before and after annealing for 40 min at 330 °C on an InGaAs quantum well grown on an InP (001) substrate and capped with a 20 nm-thick As layer. Inset: STM image of the InGaAs (001) surface after the sample preparation. Feedback parameters: $V_s = +1.3$ V, $I_t = 100$ pA, and temperature of 77 K.

Upon annealing of the InP sample at 330 °C for 30 min, all the peaks related to the amorphous arsenic layer decrease and a new small peak appears at 346 cm⁻¹ [labeled LO_{InP} in Fig. 3(a)]. After two additional hours of annealing at 330 °C, this peak has significantly increased, while the doublet peak has almost vanished, indicating the sublimation of the As capping layer. Additional features are then visible in Fig. 4(a). The main peak shows a shoulder at low wave numbers centered at 305 cm⁻¹ and a tail at higher wave numbers. Three small peaks are also measured between 600 and 700 cm⁻¹. All the peaks are the signature of InP phonon lines and are, respectively, assigned to the transverse optical (TO) (305 cm⁻¹), longitudinal optical (LO) (346 cm⁻¹), 2TO (625 cm⁻¹),

TO + LO (655 cm⁻¹), and 2LO (693 cm⁻¹) phonon modes.^{10,43,44} Below 200 cm⁻¹, a broad feature is still observed after sublimation and identified to the acoustic phonon modes of InP.⁴⁵ TO modes are normally forbidden when (001) substrates are analyzed using backscattering optical signals, but a slight deviation from perfect backscattering, which is caused by a small misalignment between the laser beam and the sample stage, accounts for the breakdown of the selection rules. We note that the doping level is not high enough to attribute the peak measured at 305 cm⁻¹ to the coupled LO phonon-plasmon mode.⁴⁶

Having determined the Raman peaks related to the InP bulk substrate, we now turn to the Raman peaks observed after the sublimation of the As capping layer from the In_{0.53}Ga_{0.47}As quantum well at 330 °C for 40 min. The corresponding spectrum in Fig. 4(b) shows a new intense doublet peak, which was not present on spectrum acquired prior to the sublimation. Although the peak looks different from the doublet peak measured for amorphous As, the surface of the quantum well was analyzed with STM to ensure that the As capping layer was completely removed. Performed in the same UHV system, the STM characterization reveals the presence of terraces on the whole surface of the sample. As shown in the inset of Fig. 4(b), an atomic-scale STM image shows three terraces with a height difference of 2.9 Å, corresponding to the atomic bi-layer thickness in In_{0.53}Ga_{0.47}As (001) crystals.³⁹ Each terrace consists of parallel rows separated by 1.7 nm, which corresponds to the distance between the rows of the As dimers of the As-rich (2 × 4) reconstructed surface. Therefore, the new doublet peak arises from Raman scattering caused by phonon excitations in the In_{0.53}Ga_{0.47}As quantum well.

The peaks at small (236 cm⁻¹) and high (267 cm⁻¹) wave numbers are assigned to the InAs-like and GaAs-like LO phonons, consistent with the literature.⁴⁷ Due to the experimental configuration, which involves Raman measurements in a backscattering arrangement, the TO modes should not contribute to the signal, except for slight misorientation of the sample or scattering processes, such as alloy disorder, that break the wave vector conservation.⁴⁸ Similar to the InP substrate, where the TO phonon mode was observed, we believe that the TO phonon mode contributes to the linewidth of the doublet peak.⁴⁹ At lower wave numbers, below 200 cm⁻¹, the broad and featureless peak is identified as disorder-activated acoustic phonon modes,^{47,48} whereas at higher wave numbers, in the range between 425 and 560 cm⁻¹, the second-order optical phonon modes are barely resolved.⁴⁷ This band has also been shown to reflect the doping level of the In_{0.53}Ga_{0.47}As quantum well.^{50,51} However, based on the rather high wave number of the InAs-like LO phonon⁵¹ and the analysis of the position of the Fermi level with ultraviolet photoemission spectroscopy and scanning tunneling spectroscopy,³⁹ we rule out an accumulation of electrons at the surface of the quantum well. The Raman peaks measured in the spectra are, therefore, consistent with the preparation of a clean and well-ordered In_{0.53}Ga_{0.47}As (001) surface, where the Fermi level is pinned midgap.

B. InSb surfaces

InSb is a material of choice for near-infrared and mid-wave infrared applications.⁵² For the past decade, the material has regained new interest because of the strong spin-orbit coupling,

which, when combined with proximity-induced superconductivity from a parent superconductor, is essential for the exploration of topological superconductivity.^{53,54} For these studies, the quality of the induced superconducting gap critically depends on the atomic scale uniformity of the semiconductor/metal interfaces. It is, therefore, essential to start from clean and reconstructed InSb surfaces to grow highly ordered epitaxial interfaces, where the crystallinity of both the semiconductor and the metal components is maintained.

To obtain high-quality InSb surfaces, the thin native oxide can be removed by eroding the surface with atomic hydrogen, with the InSb crystal kept at a temperature of 200 °C in UHV. The Raman spectrum measured before the desorption of the thin native oxide layer on an InSb (001) surface is shown in Fig. 5(a). Due to the small thickness of the oxide layer, an intense peak is observed at 190 cm^{-1} and corresponds to the LO phonon line of bulk InSb. Its linewidth is broad and could include a small contribution of the TO phonon line (180 cm^{-1}) because the incident light is not exactly normal to the surface. It is surrounded by several smaller peaks that are, respectively, attributed to the 2TA (117 cm^{-1}), 2TO (362 cm^{-1}), and 2LO (381 cm^{-1}) phonon modes.^{55,56} An additional peak is visible at 298 cm^{-1} . This peak could arise from scattering processes involving both TA and TO phonons⁵⁵ but also from phonon modes in the $\text{Al}_{0.3}\text{In}_{0.7}\text{Sb}$ barrier.^{57,58} Similar measurements performed with the InSb (001) substrate only reveal the absence of the peak (inset of Fig. 5), consistent with previous studies of bulk InSb.⁵⁹ Therefore, it is caused by the AlSb-like LO phonons, despite a depth of the barrier, which is at the limit of the probe depth measured by Raman spectroscopy at a wavelength of 532 nm.⁶⁰

As this feature corresponds to a signal from the bulk, which is not likely to change when the InSb (001) surface is modified, the AlSb-like LO phonon line is taken as a reference. Eroding the native oxide with hydrogen leads to a red shift of the main peak. At the end of the oxide removal, the STM image of the surface shows a clean and well-ordered surface, with the formation of the $c(2 \times 8)$ reconstruction [Fig. 5(b)]. This wave number corresponds to the energy of the loss peak measured with High Resolution Energy Electron Loss Spectroscopy (HREELS) on the $c(2 \times 8)$ reconstructed InSb (001) surface.^{61,62} It is assigned to the Fuchs–Kliwer surface phonon mode of InSb.⁶³ Therefore, the shift of the main line upon oxide removal indicates an increasing contribution from the surface phonon mode with respect to the bulk LO phonon line of InSb. We note that this significant change takes along with a more subtle change observed below 100 cm^{-1} , where a small peak pointed by an arrow in Fig. 5(a) emerges at 84 cm^{-1} , in the wave number region corresponding to the 2TA phonon modes.

To assess the importance of the surface structure on the detection of the surface phonon mode, the InSb (111) surface was also investigated. As shown in Fig. 6, the [111] orientation favors the contribution of the TO phonon mode, which is the main line measured at 180 cm^{-1} , whatever the state of the surface is. A small shoulder is visible at a higher wave number and is attributed to the LO phonon line. A small but broad peak is observed in the region between 350 and 382 cm^{-1} . It is caused by scattering processes involving the 2TO and 2LO phonon modes, in agreement with the overtones found in the InSb (001) layer. A small but narrower peak is measured

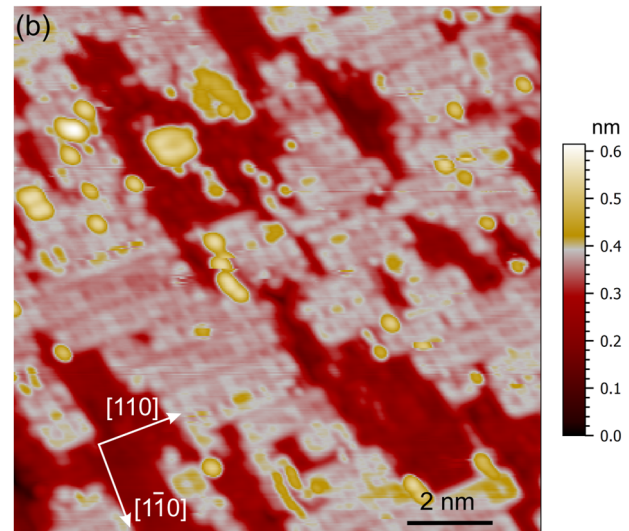
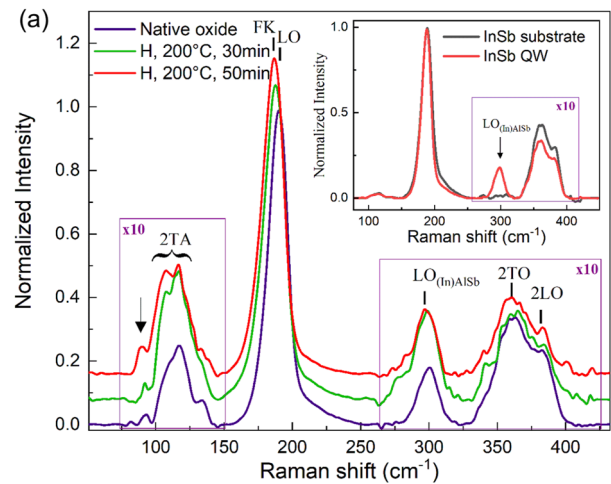


FIG. 5. (a) Evolution of the Raman spectra measured on an InSb/InAlSb/InSb (001) heterostructure upon simultaneous annealing and hydrogen sputtering of the sample. The transverse acoustic, the transverse and longitudinal optical, and the Fuchs–Kliwer surface phonon modes are labeled TA, TO, LO, and FK, respectively. The spectra are vertically shifted for convenience. (b) STM image of the In-rich $c(2 \times 8)$ InSb (001) surface after the second preparation step. Feedback parameters: $V_s = -2.0$ V, $I_t = 120$ pA, and temperature of 77 K. The color scale has been chosen to highlight the faint contrast of the $c(2 \times 8)$ reconstruction.

in between, at 305 cm^{-1} . It is assigned to the TO phonon of the InP (111) substrate, despite its depth, 30 nm underneath the InSb surface. Upon removal of the oxide layer, as demonstrated by the observation of an In-rich (3×3) reconstruction with STM,⁶⁴ the InSb-related phonon lines do not shift. The removal of the oxide layer is detected through an increase in the TO peak intensity and a slight decrease in the signal at the edge of this peak at higher wave numbers. However, the surface optical phonon of the InSb (111) surface is not resolved. Positioned between the TO and LO phonon modes,⁶⁵ it overlaps with both modes, which makes its detection

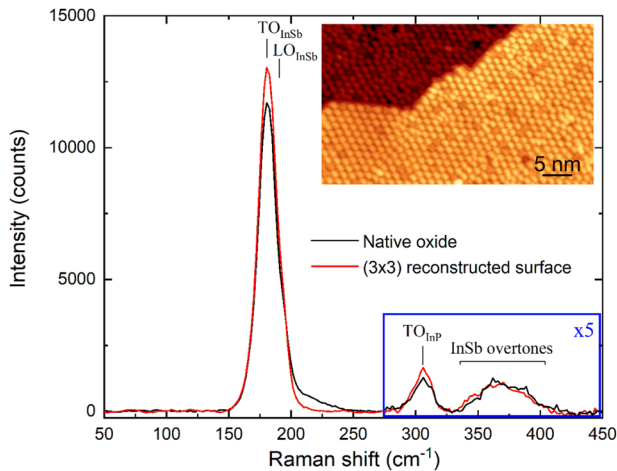


FIG. 6. Evolution of the Raman spectra measured on an InSb/InP (111) heterostructure upon simultaneous annealing and hydrogen sputtering of the sample for 60 min at 300 °C. The transverse and longitudinal optical phonon modes are labeled TO and LO, respectively. Inset: STM image of the InSb (111) surface showing a (3 × 3) reconstruction after the sample preparation. Feedback parameters: $V_s = -1.8$ V, $I_t = 150$ pA, and temperature of 77 K.

more difficult than for the (001) surface, where the contribution of the TO mode is negligible.

IV. CONCLUSION

In summary, a Raman apparatus compatible with the constraints imposed by the UHV environment has been built. It relies on the use of a fiber optic probe where the aspheric lens, which collects the backscattered photons, is located in the UHV chamber. This geometry enables the use of a lens with a diameter of 10 mm, providing an effective numerical aperture of 0.4. As a result, the Raman intensity of thin semiconductor layers is detected with high spectral quality for acquisition times about a few minutes. The system has been tested for the preparation of III–V semiconductor surfaces, which aims at recovering the atomic structure of the sample surface. The comparison of the Raman spectra measured in the course of the cleaning process with atomically resolved STM images of the surfaces shows that Raman spectroscopy, as a non-invasive and fast chemical analysis technique, gives good complementary information about the surface preparation of III–V semiconductors. Despite the weakness of the Raman effect, overtones and surface phonon modes have been measured, indicating that the sensitivity of the measurements is suitable for the future study of atomically thin two-dimensional materials in UHV.

ACKNOWLEDGMENTS

This study was financially supported by the REGION Hauts-de-France (Equipes mixtes Grant No. LS 150313 and STARS Grant No. 20.01544/3), the French National Research Agency (INSPIRING Project No. ANR-21-CE09-0026-01), and the IEMN CMNF and PCMP-PCP platforms of the RENATECH network.

AUTHOR DECLARATIONS

Conflict of Interest

The authors have no conflicts to disclose.

Author Contributions

Wijden Khelifi: Conceptualization (lead); Data curation (equal); Formal analysis (equal); Investigation (lead). **Damien Cannesson:** Resources (supporting). **Maxime Berthe:** Resources (supporting); Software (supporting); Supervision (supporting). **Sébastien Legendre:** Resources (supporting). **Christophe Coinon:** Resources (supporting). **Ludovic Desplanque:** Conceptualization (equal); Resources (equal). **Xavier Wallart:** Supervision (supporting); Validation (supporting). **Louis Biadala:** Supervision (supporting). **Bruno Grandidier:** Supervision (equal); Writing – original draft (equal). **Pierre Capiod:** Data curation (equal); Formal analysis (equal); Investigation (supporting); Supervision (equal); Writing – original draft (equal).

DATA AVAILABILITY

The data that support the finding of this study are available from the corresponding author upon request.

REFERENCES

- I. Zardo, S. Conesa-Boj, F. Peiro, J. R. Morante, J. Arbiol, E. Uccelli, G. Abstreiter, and A. Fontcuberta i Morral, *Phys. Rev. B* **80**, 245324 (2009).
- P. H. Tan, K. Brunner, D. Bougeard, and G. Abstreiter, *Phys. Rev. B* **68**, 125302 (2003).
- N. H. Nickel, P. Lengsfeld, and I. Sieber, *Phys. Rev. B* **61**, 15558–15561 (2000).
- H. Li, Q. Zhang, C. C. R. Yap, B. K. Tay, T. H. T. Edwin, A. Olivier, and D. Baillargeat, *Adv. Funct. Mater.* **22**, 1385–1390 (2012).
- Y. Wang, C. Cong, C. Qiu, and T. Yu, *Small* **9**, 2857–2861 (2013).
- B. Chakraborty, H. S. S. R. Matte, A. K. Sood, and C. N. R. Rao, *J. Raman Spectrosc.* **44**, 92–96 (2012).
- D. Wolverson, S. Crampin, A. S. Kazemi, A. Ilie, and S. J. Bending, *ACS Nano* **8**, 11154–11164 (2014).
- X. Zhang, X.-F. Qiao, W. Shi, J.-B. Wu, D.-S. Jiang, and P.-H. Tan, *Chem. Soc. Rev.* **44**, 2757–2785 (2015).
- H. B. Ribeiro, M. A. Pimenta, and C. J. de Matos, *J. Raman Spectrosc.* **49**, 76–90 (2017).
- J.-M. Jin, M. W. C. Dharma-wardana, D. J. Lockwood, G. C. Aers, Z. H. Lu, and L. J. Lewis, *Phys. Rev. Lett.* **75**, 878–881 (1995).
- K. Hinrichs, A. Schierhorn, P. Haier, N. Esser, W. Richter, and J. Sahm, *Phys. Rev. Lett.* **79**, 1094–1097 (1997).
- J. Zhuang, X. Xu, Y. Du, K. Wu, L. Chen, W. Hao, J. Wang, W. K. Yeoh, X. Wang, and S. X. Dou, *Phys. Rev. B* **91**, 161409 (2015).
- S. Sheng, J.-B. Wu, X. Cong, Q. Zhong, W. Li, W. Hu, J. Gou, P. Cheng, P.-H. Tan, L. Chen, and K. Wu, *ACS Nano* **13**, 4133–4139 (2019).
- M. Sun, Y. Fang, Z. Zhang, and H. Xu, *Phys. Rev. E* **87**, 020401 (2013).
- R. Zhang, Y. Zhang, Z. C. Dong, S. Jiang, C. Zhang, L. G. Chen, L. Zhang, Y. Liao, J. Aizpurua, Y. Luo *et al.*, *Nature* **498**, 82–86 (2013).
- J. M. Klingsporn, N. Jiang, E. A. Pozzi, M. D. Sonntag, D. Chulhai, T. Seideman, L. Jensen, M. C. Hersam, and R. P. V. Duyne, *J. Am. Chem. Soc.* **136**, 3881–3887 (2014).
- N. Tallarida, L. Rios, V. A. Apkarian, and J. Lee, *Nano Lett.* **15**, 6386–6394 (2015).

- ¹⁸E. A. Pozzi, G. Goubert, N. Chiang, N. Jiang, C. T. Chapman, M. O. McAnally, A.-I. Henry, T. Seideman, G. C. Schatz, M. C. Hersam, and R. P. V. Duyne, *Chem. Rev.* **117**, 4961–4982 (2016).
- ¹⁹M. G. Hell, N. Ehlen, B. V. Senkovskiy, E. H. Hasdeo, A. Fedorov, D. Domrowski, C. Busse, T. Michely, G. di Santo, L. Petaccia *et al.*, *Nano Lett.* **18**, 6045–6056 (2018).
- ²⁰S. Sheng, W. Li, J. Gou, P. Cheng, L. Chen, and K. Wu, *Rev. Sci. Instrum.* **89**, 053107 (2018).
- ²¹G. Laurence, F. Simondet, and P. Saget, *Appl. Phys.* **19**, 63–70 (1979).
- ²²M. Fahed, L. Desplanque, D. Troadec, G. Patriarche, and X. Wallart, *Nanotechnology* **27**, 505301 (2016).
- ²³G. Bell, N. Kaijaks, R. Dixon, and C. McConville, *Surf. Sci.* **401**, 125–137 (1998).
- ²⁴J. L. Webb, J. Knutsson, M. Hjort, S. Gorji Ghalamestani, K. A. Dick, R. Timm, and A. Mikkelsen, *Nano Lett.* **15**, 4865–4875 (2015).
- ²⁵T. Xu, K. A. Dick, S. Plissard, T. H. Nguyen, Y. Makoudi, M. Berthe, J.-P. Nys, X. Wallart, B. Grandidier, and P. Caroff, *Nanotechnology* **23**, 095702 (2012).
- ²⁶N. A. Franchina Vergel, L. C. Post, D. Sciacca, M. Berthe, F. Vaurette, Y. Lambert, D. Yarekha, D. Troadec, C. Coinon, G. Fleury *et al.*, *Nano Lett.* **21**, 680–685 (2021).
- ²⁷A. D. Álvarez, T. Zhu, J. Nys, M. Berthe, M. Empis, J. Schreiber, B. Grandidier, and T. Xu, *Surf. Sci.* **653**, 92–96 (2016).
- ²⁸U. Resch, S. M. Scholz, U. Rossow, A. B. Müller, W. Richter, and A. Förster, *Appl. Surf. Sci.* **63**, 106–110 (1993).
- ²⁹E. D. Palik, *Handbook of Optical Constants of Solids* (Academic Press, Orlando, 1985).
- ³⁰A. Díaz Álvarez, N. Peric, N. A. Franchina Vergel, J.-P. Nys, M. Berthe, G. Patriarche, J.-C. Harmand, P. Caroff, S. Plissard, P. Ebert *et al.*, *Nanotechnology* **30**, 324002 (2019).
- ³¹L. He, L. E. Clinger, and C. J. K. Richardson, *J. Vac. Sci. Technol., B: Nanotechnol. Microelectron.: Mater., Process., Meas., Phenom.* **31**, 061204 (2013).
- ³²M. Fahed, L. Desplanque, C. Coinon, D. Troadec, and X. Wallart, *Nanotechnology* **26**, 295301 (2015).
- ³³Y.-P. Liu, S. Yngman, A. Troian, G. D’Acunto, A. Jönsson, J. Svensson, A. Mikkelsen, L.-E. Wernersson, and R. Timm, *Appl. Surf. Sci.* **593**, 153336 (2022).
- ³⁴D. Caffin *et al.*, *J. Vac. Sci. Technol., B: Nanotechnol. Microelectron.: Mater., Process., Meas., Phenom.* **15**, 854 (1997).
- ³⁵J. A. del Alamo, *Nature* **479**, 317–323 (2011).
- ³⁶G. Ribordy, N. Gisin, O. Guinnard, D. Stuck, M. Wegmuller, and H. Zbinden, *J. Mod. Opt.* **51**, 1381–1398 (2004).
- ³⁷N. Namekata, S. Sasamori, and S. Inoue, *Opt. Express* **14**, 10043–10049 (2006).
- ³⁸L. Seravalli, G. Trevisi, P. Frigeri, D. Rivas, G. Muñoz-Matutano, I. Suárez, B. Alén, J. Canet-Ferrer, and J. P. Martínez-Pastor, *Appl. Phys. Lett.* **98**, 173112 (2011).
- ³⁹N. A. Franchina Vergel, A. Tadjine, V. Notot, M. Mohr, A. Kouassi N’Guissan, C. Coinon, M. Berthe, L. Biadala, K. K. Sossoe, M. M. Dzagli *et al.*, *Phys. Rev. Mater.* **3**, 094604 (2019).
- ⁴⁰N. Peric, C. Durand, M. Berthe, Y. Lu, K. N’Konou, R. Coratger, I. Lefebvre, P. Ebert, L. Biadala, L. Desplanque *et al.*, *Appl. Phys. Lett.* **121**, 192104 (2022).
- ⁴¹J. S. Lannin, *Phys. Rev. B* **15**, 3863–3871 (1977).
- ⁴²H. Wilhelm, W. Richter, U. Rossow, D. Zahn, D. Woolf, D. Westwood, and R. Williams, *Surf. Sci.* **251–252**, 556–560 (1991).
- ⁴³E. Bedel, G. Landa, R. Carles, J. B. Renucci, J. M. Roquais, and P. N. Favenec, *J. Appl. Phys.* **60**, 1980–1984 (1986).
- ⁴⁴M. Sinyukov, R. Trommer, and M. Cardona, *Phys. Stat. Sol.* **86**, 563–568 (1978).
- ⁴⁵E. Bedel, G. Landa, R. Carles, J. P. Redoules, and J. B. Renucci, *J. Phys. C: Solid State Phys.* **19**, 1471–1479 (1986).
- ⁴⁶R. Fukasawa and S. Perkowitz, *Phys. Rev. B* **50**, 14119–14124 (1994).
- ⁴⁷Z. C. Feng, A. A. Allerman, P. A. Barnes, and S. Perkowitz, *Appl. Phys. Lett.* **60**, 1848–1850 (1992).
- ⁴⁸K. Kakimoto and T. Katoda, *Appl. Phys. Lett.* **40**, 826–828 (1982).
- ⁴⁹T. P. Pearsall, R. Carles, and J. C. Portal, *Appl. Phys. Lett.* **42**, 436–438 (1983).
- ⁵⁰N. Matruillo, M. Constant, G. Sagon, R. Fauquembergue, and A. Leroy, *J. Raman Spectrosc.* **26**, 167–172 (1995).
- ⁵¹K. Radhakrishnan, T. H. K. Patrick, H. Q. Zheng, P. H. Zhang, and S. F. Yoon, *J. Vac. Sci. Technol., A* **18**, 713–716 (2000).
- ⁵²B. W. Jia, K. H. Tan, W. K. Loke, S. Wicaksono, K. H. Lee, and S. F. Yoon, *ACS Photonics* **5**, 1512–1520 (2018).
- ⁵³M. Pendharkar, B. Zhang, H. Wu, A. Zarassi, P. Zhang, C. P. Dempsey, J. S. Lee, S. D. Harrington, G. Badawy, S. Gazibegovic *et al.*, *Science* **372**, 508–511 (2021).
- ⁵⁴M. T. Deng, C. L. Yu, G. Y. Huang, M. Larsson, P. Caroff, and H. Q. Xu, *Nano Lett.* **12**, 6414–6419 (2012).
- ⁵⁵W. Kiefer, W. Richter, and M. Cardona, *Phys. Rev. B* **12**, 2346–2354 (1975).
- ⁵⁶C. Seok, M. Choi, S. Park, J. Jung, Y. Park, I.-S. Yang, and E. Yoon, *ECS Solid State Lett.* **3**, P27–P29 (2013).
- ⁵⁷V. P. Gnezdilov, D. J. Lockwood, and J. B. Webb, *Phys. Rev. B* **48**, 11228–11233 (1993).
- ⁵⁸J. B. Webb, D. Lockwood, and V. Gnezdilov, *J. Cryst. Growth* **137**, 405–414 (1994).
- ⁵⁹V. P. Gnezdilov, D. J. Lockwood, and J. B. Webb, *Phys. Rev. B* **48**, 11234–11239 (1993).
- ⁶⁰E. D. Palik, *Handbook of Optical Constants of Solids* (Academic Press, 1998), Vol. 3.
- ⁶¹S. Evans, L. Cao, R. Egdell, R. Droopad, S. Parker, and R. Stradling, *Surf. Sci.* **226**, 169–179 (1990).
- ⁶²T. Jones, M. Ding, N. Richardson, and C. McConville, *Appl. Surf. Sci.* **45**, 85–90 (1990).
- ⁶³R. Fuchs and K. L. Kliewer, *Phys. Rev.* **140**, A2076–A2088 (1965).
- ⁶⁴J. Mäkelä, Z. S. Jahanshah Rad, J.-P. Lehtiö, M. Kuzmin, M. P. J. Punkkinen, P. Laukkanen, and K. Kokko, *Sci. Rep.* **8**, 14382 (2018).
- ⁶⁵I. Hernández-Calderón, *Surf. Sci.* **152–153**, 1130–1134 (1985).